Electronic and magnetic state of $LaMnO_3$ epitaxially strained on $SrTiO_3$: Effect of local correlation and nonlocal exchange

Hrishit Banerjee,[1] Oleg Janson,[2,3] Karsten Held,[3] and Tanusri Saha-Dasgupta[4,5,*]
[1] *Insitut für Theoretische Physik–Computational Physics, TU Graz, Petersgaße 16, Graz 8010, Austria*
[2] *Institute for Theoretical Solid State Physics, IFW Dresden, Helmholtzstraße 20, 01069 Dresden, Germany*
[3] *Institut für Festkörperphysik, TU Wien, Wiedner Hauptstraße 8-10, Vienna, Austria*
[4] *S. N. Bose National Centre for Basic Sciences, JD Block, Sector III, Salt Lake, Kolkata, West Bengal 700106, India*
[5] *Indian Association for the Cultivation of Science, 2A & 2B, Raja Subodh Chandra Mallick Rd., Jadavpur, Kolkata, West Bengal 700032, India*

(Received 27 July 2019; published 18 September 2019)

Motivated by the puzzling report of the observation of a ferromagnetic insulating state in $LaMnO_3/SrTiO_3$ heterostructures, we calculate the electronic and magnetic state of $LaMnO_3$, coherently matched to a $SrTiO_3$ square substrate within a "strained-bulk" geometry. We employ three different density functional theory based computational approaches: (a) density functional theory (DFT) supplemented with Hubbard U (DFT + U), (b) DFT + dynamical mean-field theory (DMFT), and (c) a hybrid functional treatment of the exchange-correlation functional. While the first two approaches include local correlations and exchange at Mn sites, treated in a static and dynamic manner, respectively, the last one takes into account the effect of nonlocal exchange at all sites. We find in all three approaches that the compressive strain induced by the square substrate of $SrTiO_3$ turns $LaMnO_3$, from an antiferromagnet with sizable orbital polarization, to a ferromagnet with suppressed Jahn-Teller distortion, in agreement with experiment. However, while both DFT + U and DFT + DMFT provide a metallic solution, only the hybrid calculations result in an insulating solution, as observed in experiment. This insulating behavior is found to originate from an electronic charge disproportionation. Our conclusions remain valid when we investigate $LaMnO_3/SrTiO_3$ within the experimental setup of a superlattice geometry using DFT + U and hybrid calculations.

DOI: 10.1103/PhysRevB.100.115143

I. INTRODUCTION

In recent times the study of interfaces formed between perovskite oxides has made a deep impact on the community engaged in both theoretical and experimental condensed matter research. The presence of a highly conducting two-dimensional electron gas (2DEG) at the interface between oxide insulators grown along the [001] direction, has opened a road to many different prospective device applications. Interfaces have been formed between band insulators, like between $LaAlO_3$ (LAO) and $SrTiO_3$ (STO) [1], generating significant excitement at the 2DEG interface [2]. This excitement has been propagated further in terms of synthesis of interfaces between Mott insulators and band insulators, as in the case of $GdTiO_3$ (GTO) and $SrTiO_3$ [3], or $LaTiO_3$ and $SrTiO_3$ [1]. The behavior of the GTO/STO interface has been found to be qualitatively different from that of the LAO/STO interface in terms of the absence of a critical thickness for metallicity; and the carrier density of the 2DEG being in perfect agreement with that expected from polar charge [4]. The qualitatively different behavior of the two systems has been rationalized by the fact that the gap in $GdTiO_3$ being a Mott gap arises within the Ti d manifold, while that in $LaAlO_3$ arises between filled O p bands and empty Al bands, thereby influencing the band alignment in a qualitative manner [5].

Given the dissimilar behavior of band and Mott insulators in oxide heterostructures, it is curious to ask what happens if an insulator such as $LaMnO_3$ (LMO) featuring a cooperative Jahn-Teller (JT) distortion of MnO_6 octahedra along with the strong on-site repulsion, is brought in contact with the band insulator $SrTiO_3$. The influence of structural distortions is expected to be qualitative in this case, though LAO, GTO, and LMO all belong to the same polar family. Indeed, LMO/STO heterostructures have been synthesized and probed experimentally to characterize the nature of the interfaces, formed between LMO and STO. The varied nature of magnetic and electronic behavior of the LMO/STO interfaces has been reported, depending on the relative thickness of LMO and STO and their geometry [6–12]. Among all, the most intriguing is the suggestion of ferromagnetic insulating behavior, which has been reported for LMO/STO superlattices when LMO and STO have comparable thicknesses [12], as well as in thin-film/substrate geometries [10]. This is counterintuitive, since ferromagnetism is commonly associated with metallicity and antiferromagnetism is typical for insulators. Some attempts have been made to justify the observed coexistence of ferromagnetism and insulating nature. One of them involved Monte Carlo simulation [12] of a double-exchange model, with orbital polarization to explain the behavior. However, experimental investigation shows significant suppression of the JT distortion [12] in the superlattice geometry showing ferromagnetic insulating behavior, and thus the orbital polarization is also expected to be suppressed. The other one

---

[*] t.sahadasgupta@gmail.com

relies on the concept of electronic phase separation leading to nucleation of metallic nanoscale ferromagnetic islands embedded in an insulating antiferromagnetic matrix, which gives rise to both ferromagnetic signal and insulating resistivity [10]. For this scenario to be valid, the polar charge created at the interface, must reside at the LMO side, resulting in doping of LMO. The direction of charge transfer, however, has not been established so far. The observed coexistence of ferromagnetism and insulating nature at the LMO/STO interface thus remains a puzzle. Is it intrinsic or due to extrinsic reasons such as deviations from stoichiometry in the heterostructure, the presence of defects that trap the free carriers, or inhomogeneity of the samples?

Investigations using density functional theory (DFT) supplemented with Hubbard U (DFT + U) on strained LMO corresponding to that of STO showed [13] a suppression of the JT distortion and a ferromagnetic ground state, which is albeit metallic rather than insulating as claimed in experiments. In a further DFT + U study of LMO strained to STO [14], the structural relaxation allowing for symmetry lowering to monoclinic structure, and resultant antiferro-orbital ordering between symmetry inequivalent Mn atoms was used to explain the ferromagnetic insulating behavior of LMO. However, such symmetry lowering may be difficult to be accommodated within a heterostructure geometry, where LMO might be sandwiched between the layers of STO, thus being constrained from both top and bottom and unable to deviate from the cubic group of symmetry.

In view of the above, we revisit the problem considering three different computational approaches on bulk LMO with its in-plane lattice constants constrained to that corresponding to a square substrate geometry of STO. We consider the general framework of DFT, which is expected to capture the structural changes that happen upon epitaxial straining of LMO correctly. To take into account the strong correlation effect at the transition metal (TM) site, which is known to be essential in proper description of magnetic and electronic ground states of manganites, we follow three different methods: (i) The static treatment of correlations including an orbital-dependent potential that is parametrized in terms of Hubbard parameter U and Hund parameter J_H within the DFT + U formulation [15] as followed in previous literature [13,14]. (ii) Hybrid functional as implemented by Heyd-Scuseria-Ernzerhof (HSE) [16] in which a portion of the exact nonlocal Hartree-Fock (HF) exchange is mixed with the complementary DFT in local [local density approximation (LDA)] or semilocal [generalized gradient approximation (GGA)] approximated exchange. As opposed to the "+U" formulation where the improved treatment of exchange effects is limited to the partially filled TM sites, the hybrid functional approach uses an orbital-dependent functional acting on all states, extended as well as localized. It thus has an impact on both TM sites and O sites. This may become important in strongly covalent systems as manganites. Indeed, as argued in Ref. [22] the bulk properties of LMO are reproduced better in hybrid calculation, compared to DFT + U. (iii) DFT+dynamical mean field theory (DMFT) [17] in order to probe the effect of dynamical correlation as well as that of temperature. In order to minimize the computational effort, the DMFT calculations were carried out employing the Mn d only low-energy Hamiltonian, consisting of five orbitals per Mn site, derived out of DFT in the maximally localized Wannier function basis. Such a DMFT treatment does not account for charge redistribution between the TM and ligand sites, as well as for correlation effects on the latter.

We find a ferromagnetic ground state in all three approaches, driven by the marked reduction of orthorhombic distortion in the optimized LMO structure when epitaxially strained to the square substrate of STO, resulting in a strong suppression of the JT distortion. The suppression of the JT distortion and modification of the octahedral rotation, as captured in our study, is in agreement with the structural characterization of LMO/STO superlattices [12], stressing once again the accuracy of DFT in addressing the structural properties. Although the three methods agree on the magnetic state of strained LMO, the DFT + U and DFT + DMFT resulted in metallic solutions, while the treatment of the correlation effect within the hybrid functional resulted in an insulating solution. This surprising result of ferromagnetic insulating solution within hybrid calculations, was traced to originate from electronically driven charge disproportion within the Mn sublattice that arises due to a strain-driven enhanced covalency between Mn and O. We note that in the hybrid approach, as opposed to both DFT + U and DFT + DMFT, the exact exchange is calculated for all the orbitals, not only for the TM sites. This, in turn, presumably highlights the Mn-O covalency effect, and thus the importance of correlation effects on the O p states, which are considered uncorrelated or with no self-energy in the conventional DFT + U and in the noncharge self-consistent version of the Mn d only DFT + DMFT setup, used in the present study.

Finally, in order to further probe the effect of the heterostructure geometry, as in the experimental setup, we compare the results of DFT + U and hybrid calculations for $(\mathrm{LMO})_{4.5}/(\mathrm{STO})_{4.5}$ with two symmetric n-type interfaces in superlattice geometry, which takes into account the presence of STO in an explicit manner. The calculations on heterostructure geometry confirm the ferromagnetic insulating result for the hybrid and ferromagnetic metallic state for the DFT + U approach, making our conclusion remain valid even in experimentally relevant geometry. We hope that our extensive theoretical study will regenerate interest in the curious case of the ferromagnetic insulating state of the LMO/STO interface, in terms of better characterization of the samples with detailed knowledge on oxygen vacancies, defects, and inhomogeneities on one hand, and a more complete many-body treatment taking into account the oxygen orbitals explicitly within a charge self-consistent scheme on the other.

II. COMPUTATIONAL DETAILS

Our DFT calculations were carried out in a plane-wave basis with projector-augmented wave (PAW) potentials [18] as implemented in the Vienna Ab initio Simulation Package (VASP) [19,20]. The DFT exchange-correlation functional was chosen to be that given by GGA, implemented following the Perdew-Burke-Ernzerhof (PBE) prescription [21]. For ionic relaxations, internal positions of the atoms were allowed to relax until the forces became less than 0.005 eV/Å. An energy cutoff of 550 eV, and 5 × 5 × 3 Monkhorst-Pack

k-points mesh were found to provide a good convergence of the total energy in self-consistent field calculations. The plane-wave cutoff and the k-point mesh have been checked for convergence of the obtained results. PAW-PBE potentials with highest available energy cutoff of 220 eV for La (11 valence e^-), 270 eV for Mn (13 valence e^-), and 400 eV for O (6 valence e^-) have been used.

The DFT + U calculations were carried out in the form of GGA + U. The value of U at the Mn sites in the GGA + U scheme was varied from 2 to 8 eV; and a U value of 3.5 eV was found to be adequate to reproduce the experimentally observed insulating A-type antiferromagnetic (A-AFM) nature of bulk unstrained LaMnO$_3$. The Hund's coupling parameter J_H was chosen be 0.9 eV.

The functional used in hybrid calculation can be mathematically expressed as

$$E_{XC}^{\mathrm{HSE}}(\omega) = \alpha E_X^{\mathrm{HF,SR}}(\omega) + (1-\alpha)E_X^{\mathrm{PBE,SR}}(\omega) + E_X^{\mathrm{PBE,LR}}(\omega) + E_C^{\mathrm{PBE}}, \quad (1)$$

where α is the mixing parameter and ω is an adjustable parameter controlling the short-rangeness of the interaction. Here $E_X^{\mathrm{HF,SR}}$ denotes the short-range HF exchange functional, $E_X^{\mathrm{PBE,SR}}$ denotes the short-range PBE exchange functional, $E_X^{\mathrm{PBE,LR}}$ indicates the long-range PBE exchange functional, and E_C^{PBE} refers to the correlation functional as given by PBE. The standard value of $\omega = 0.2$ (referred to as HSE06) along with varying values of α of 0.15, 0.20, 0.25, and 0.30 were used in our calculations. The influence of the mixing factor, α, in hybrid functionals has been systematically studied for $3d^0$–$3d^8$ transition-metal perovskites LaMO$_3$ (M = Sc-Cu) by He and Franchini [22], which concludes that for LMO the choice of $\alpha = 0.15$ reproduces the experimental band gaps, magnetic moments, and exchanges best. However the calculations by He and Franchini [22] were carried with potentials with lower cutoffs of 137 eV for La (9 valence e^-), 270 eV for Mn (7 valence e^-), and 283 eV for O (6 valence e^-), available at that time, with a maximum cutoff energy of 300 eV. Repeating the calculations using newer potentials with higher cutoff available now, as mentioned previously, we find the agreement with experimental results to be best for $\alpha = 0.25$, which is the standard hybrid functional value. In the Appendix, we show the MARE (mean absolute relative error) for the band gaps and the magnetic moments, confirming better agreement with experimental band gap and magnetic moments for $\alpha = 0.25$ compared to previously suggested [22] $\alpha = 0.15$. All calculations reported in the following, were thus carried out for a choice of α value of 0.25.

The starting point of our DFT + DMFT calculations, were GGA calculations performed in the full potential augmented plane-wave basis as implemented in WIEN2K. [23]. We used the largest possible muffin-tin radii and the basis set plane-wave cutoff as defined by $R_{\min}K_{\max} = 7$, where $R_{\min}$ is the muffin-tin radius of oxygen atoms. The consistency between plane-wave basis and augmented plane-wave basis results has been cross-checked. The Mn d band structure of a nonmagnetic GGA calculation is split into the t_{2g} and e_g manifolds, comprising 12 and 8 bands, respectively, as expected for a unit cell with with four Mn atoms and five orbitals per Mn atom. In a nonmagnetic DFT calculation, the Fermi level crosses the t_{2g} manifold, and the e_g states are empty. The maximally localized Wannier functions [24] of these five Mn d DFT orbitals were used as an input for DMFT and calculated with the WIEN2WANNIER interface [25]. As common for multisite DMFT calculations, each of the four Mn atoms in the unit cell was treated as an independent five-orbital DMFT impurity problem. Note that in contrast to earlier DMFT studies [26–28], we treated t_{2g} and e_g electrons on the same footing. Previous DFT + DMFT calculations for bulk LaMnO$_3$ employed the intraorbital Coulomb repulsion $U = 5$ eV in Refs. [26,27] or $U = 4$–7 eV in Ref. [28] with the Hund's exchange of $J = 0.75$ eV. Using these values as a starting point, we varied these parameters over a reasonable range to gain a better understanding of their influence on the physics of our five-orbital model.

The auxiliary Anderson impurity problems were solved using the continuous-time quantum Monte Carlo algorithm in the hybridization expansion [29] as implemented in W2DYNAMICS [30]. Since this algorithm scales exponentially with the number of orbitals, solving a five-orbital problem turns into a cumbersome task. To keep the impurity problem numerically tractable, we performed a calculation without charge-self-consistency [31] and employed the recently developed superstate sampling, where impurity eigenstates are grouped and each group is sampled individually [35]. The fully localized limit [36] was used as the double-counting correction. We used the rotationally invariant Kanamori interaction [37] with the intraorbital interaction $U' = U - 2J$, as commonly employed in DFT + DMFT calculations. The resulting Hamiltonian accounts for the spin flip and pair hopping terms, but neglects the different spatial extent of t_{2g} and e_g Wannier functions.

III. RESULTS

A. LMO epitaxially strained on square substrate of STO

1. *Crystal structure*

Bulk unstrained LMO grows in the orthorhombic *Pbnm* crystal structure, which is derived out of the cubic structure by expansion of the unit cell to a $\sqrt{2} \times \sqrt{2} \times 2$ perovskite supercell, resulting in four formula units in the cell, that can accommodate the GdFeO$_3$-type rotation and tilt of the oxygen octahedra as well as JT distortion. In order to mimic the effect of epitaxial strain, as in Refs. [13,14], we performed "strained-bulk" calculations, in which the structural parameters (c lattice parameter, ionic positions) of the $\sqrt{2} \times \sqrt{2} \times 2$ perovskite supercells were optimized subject to the constraint that the two in-plane lattice vectors which define the epitaxial substrate, were fixed to produce the specified square lattice of dimensions $\sqrt{2} \times a_c$, where a_c is the cubic lattice parameter corresponding to the substrate. Structural optimizations were carried out within DFT + U, and the DFT + U optimized structures have been used in all subsequent calculations.

Figure 1 shows the structure of unstrained and strained LMO viewed along the c direction. For strained calculations, we considered a range of strain values, varied over both compressive and tensile strain, from −3.4% to +2.1%. The in-plane strain produced by coherent matching of LMO to a square-lattice substrate with lattice

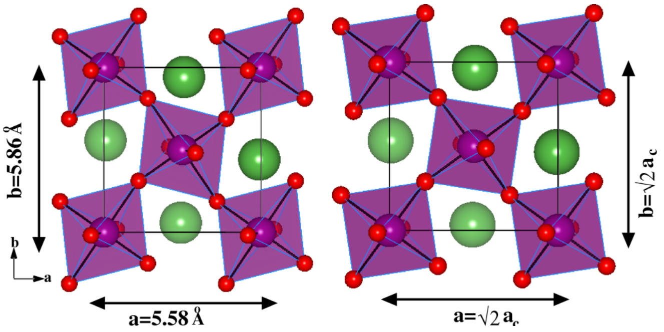

FIG. 1. The structure of unstrained (left panel) and epitaxially strained LMO to square substrate (right panel) viewed along the crystallographic c axis. Mn atoms (medium magenta balls) in octahedral coordination of O (small red balls) atoms share corners, while La atoms (large green balls) sit in voids.

parameter a_c, was quantified as $\frac{a_c-a_0}{a_0}$ with $a_0 = 3.976$ Å, the cube root of the computed volume per formula unit of the relaxed *Pbnm* structure of unstrained LMO in its lowest-energy AFM ground state of A type. Figure 2 shows the structural characteristics of the strained LMO fit to square substrate. We find a rather strong influence of straining on the structural parameters of LMO. In particular for tensile strain, the orthorhombicity of the $a = b$ structure, defined as $c/\sqrt{2}a$-1, gets strongly suppressed upon matching to a square substrate, making the structures nearly cubic (cf. top panel, Fig. 2). This also gets reflected in the JT distortion modes, defined as $Q_2 = \frac{1}{\sqrt{2}}(X_1 - X_4 - Y_2 + Y_5)$, $Q_3 = \frac{1}{\sqrt{6}}(2Z_3 - 2Z_6 - X_1 + X_4 - Y_2 + Y_5)$, with X_i, Y_i, Z_i defining oxygen coordinates of the MnO$_6$ octahedra (see Fig. 1 in Ref. [13]). Figure 2 (middle panel) shows that the JT distortion essentially vanishes for the compressive strain. Focusing on the specific case of an STO substrate, which corresponds to an a_c value of 3.905 Å and compressive strain of −1.8%, we find magnitudes of Q2 and Q3 to be 0.037 Å and 0.068 Å, respectively. The tilt and rotations are also seen to be strongly influenced by the epitaxial strain of the square substrates (cf. bottom panel, Fig. 2). Our results are in good agreement with that obtained by Lee *et al.* [13] using a similar approach.

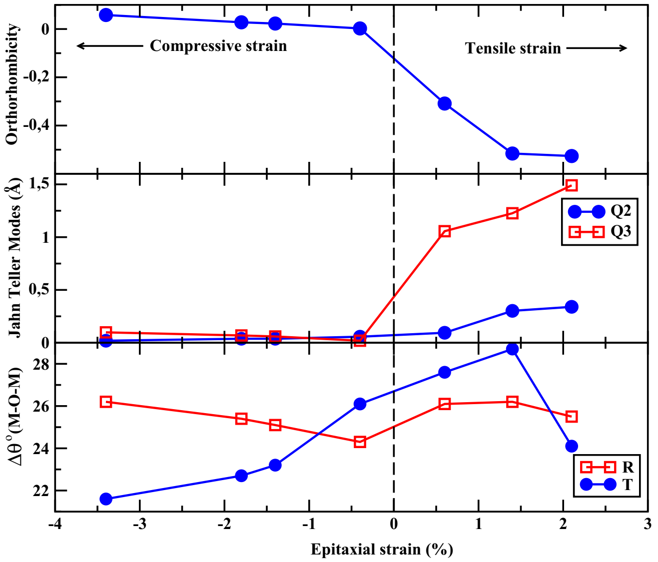

FIG. 2. The structural parameters, namely, orthorhombicity, JT distortions (Q2 and Q3), rotation (R)-tilt (T) of MnO$_6$ octahedra in the epitaxially strained bulk LMO structure.

In the following we focus on the 1.8% compressive strained LMO, as it corresponds to an STO substrate, and discuss its magnetic and electronic behavior within the framework of three approaches: DFT + U, hybrid, and DFT + DMFT.

2. *Electronic and magnetic structure:* DFT + U

We calculated the total energies of unstrained and strained LMO considering ferromagnetic (FM) and different antiferromagnetic alignment of Mn spins: A-AFM, C-AFM, and G-AFM. Here, A-AFM refers to ferromagnetic planes coupled in an antiferromagnetic manner, C-AFM refers to antiferromagnetically arranged planes coupled ferromagnetically, and G-AFM refers to antiferromagnetic alignment of Mn spins both within the plane and in the out-of-plane direction. For each of the magnetic arrangements, the structure was relaxed in order to take into account the strong influence of the structure on magnetism and vice versa. The DFT + U calculation resulted in the A-AFM insulating solution as the lowest-energy solution for the unstrained LMO, in agreement with previous studies [13,14]. The energy difference of A-AFM from FM was estimated to be small (9.01 meV/f.u.), in agreement with findings by Lee *et al.* [13] suggesting the system to be close to ferromagnetic instability which may be stabilized by external perturbation such as strain. The calculated direct band gap of 1.3 eV, estimated from band structure, is in agreement with that of Lee *et al.* [13] of 1.1 eV and Hou *et al.* [14] of 1.2 eV, which somewhat underestimates the experimental estimate [38]. The estimated in-plane and out-of-plane magnetic exchanges of 2.19 meV and −1.14 meV were also found to be in good agreement with experimental estimates of 1.85 and −1.1 meV, respectively.

Moving to strained LMO, we find the FM state to be stabilized by a large energy difference of about 175 meV/f.u. over the A-AFM state. The suppression of the JT distortion, which kills the orbital polarization, has been argued to be responsible for the observed FM behavior [13].

The left, top panel of Fig. 3 shows the DFT + U density of states (DOS), projected to d states of four Mn atoms in the unit cell, and the O p states. As seen, a DFT + U treatment of the problem results in a ferromagnetic half-metallic state, with empty Mn d states in the minority spin channel and filled Mn t_{2g} states in the majority spin channel, while partially filled Mn e_g states hybridize with O p states and cross the Fermi level. This is in agreement with the finding by Lee *et al.* [13]. The stability of half-metallic DFT + U has been checked varying the U value. An even choice of a very high value of Hubbard U ($U = 8$ eV), keeps the solution half-metallic. Interestingly, the solution is found to be half-metallic even in the GGA calculation setting $U = 0$. This is driven by the fact that the suppression of the JT distortions removes the orbital polarization, resulting in nearly degenerate e_g states, which together with the large e_g bandwidth promotes a FM spin alignment. The DFT + U method which is designed to make

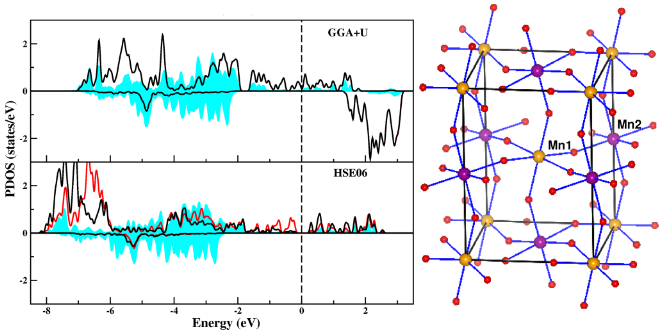

FIG. 3. Left panel: Projected density of states (PDOS) for LMO strained to an STO substrate, as calculated with DFT + U (top) and hybrid functional (bottom). The DOS projected onto the Mn d states belonging to class 1 (Mn1) and class 2 (Mn2) (see text and right panel) are shown as black and red (gray) lines, respectively; that onto O p are shown as a cyan (gray) shaded area. The zero of energy is set to Fermi energy. Right panel: The four Mn atoms in the unit cell which are structurally equivalent, however electronically form two classes within hybrid functional calculations, represented by Mn1 (yellow) and Mn2 (violet).

the configurations with larger magnetization more favorable is not effective here in a manifold of nearly degenerate bands involving only one spin channel, though the double-counting correction remains operative. The calculated moment at the Mn site turned out to be $3.86\mu_B$ with an average moment of $0.07\mu_B$ arising due to the covalency effect, setting the net moment in the cell to be an integer value of $4\mu_B$ in accordance with its half-metallic character.

3. Electronic and magnetic structure: Hybrid

Application of a hybrid functional with a choice of $\alpha = 0.25$ on unstrained bulk LMO, also correctly reproduced the experimentally observed A-AFM insulating state, with a smaller energy difference of A-AFM from FM (≈ 5 meV/f.u.) compared to that obtained in DFT + U. Our HSE06 calculation using 25% HF exchange gave a direct band gap of 1.72 eV, which is a better agreement with experimental results than DFT + U, a fact mentioned already by Munoz *et al.* [39]. The estimates of magnetic exchanges within hybrid calculation were also found to be reasonable with values of 2.46 meV and −0.60 meV for in-plane and out-of-plane exchanges.

However, qualitatively different results are obtained compared to DFT + U when the HSE06 calculations are carried out for strained LMO. Although the FM state is found to be stabilized also in hybrid calculation by an energy difference of about 90 meV/f.u. over A-AFM, this FM state is found to be insulating, as opposed to being metallic in DFT + U calculation. The DOS, as given by hybrid functional calculation, is presented in the left, bottom panel of Fig. 3.

The electronic structure is found to be markedly different from that of DFT + U on several counts. Firstly, the hybrid DOS shows a gap of about 0.3 eV, as opposed to zero gap in the case of DFT + U. Secondly, a substantial redistribution of spectral weights of O p states is observed in hybrid DOS, when compared to DFT + U. This shifts the oxygen contribution away from Fermi level. Thirdly and most remarkably, the contributions of Mn atoms turn out to be inequivalent, with two of the four Mn atoms in the cell (grouped as Mn1 in the figure shown in the right panel) occupying the body center and corners of the cell forming one class and the rest (grouped as Mn2 in the figure shown in the right panel) forming another class. The Mn2 states are found to more occupied compared to Mn1 states, suggesting a charge disproportionation between the two. To demonstrate this we calculated the Bader charge of the Mn atoms, which is considered to be a good approximation to the total electronic charge of an atom. The Bader charge calculated for Mn1 and Mn2 showed a difference of $0.07e^-$ with a difference of magnetic moment of $0.16\mu_B$; specifically Mn1 atoms have a charge $4-\delta$ and Mn2 atoms have $4+\delta$ [40].

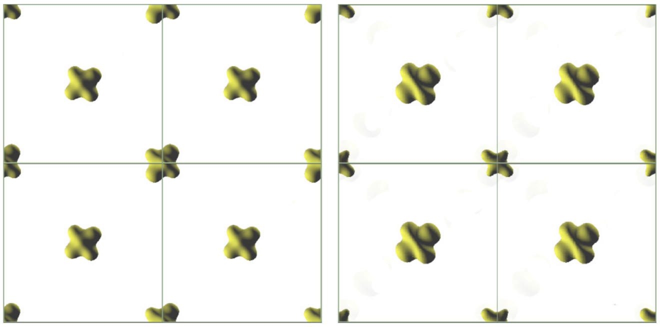

FIG. 4. Charge density of LMO epitaxially strained STO, calculated within DFT + U (left panel) and hybrid functional (right panel), viewed along the c axis. Shown are plots for the 2 × 2 supercell for better visualization. The isosurface value is set at 0.015 $e^-/\mathring{\mathrm{A}}^3$.

This is further supported by the plot of charge density in an energy window from −0.5 eV below Fermi energy up to the Fermi energy, shown in Fig. 4. While the DFT + U charge density distribution supports the ferro-orbital ordering of type $d_{3z^2-r^2} + d_{x^2-y^2}$ with no charge disproportionation between Mn atoms, as found by Hou *et al.* [14], a strong charge imbalance is noticed between Mn1 and Mn2 in the charge density plot in Fig. 4, based on the hybrid functional calculation.

We next make an attempt to understand this charge disproportionation, purely driven by an electronic mechanism as the Mn atoms are structurally equivalent within the *Pbnm* orthorhombic symmetry of the structure. We note that in $\mathrm{CaFeO_3}$ the Fe ion is in its d^4 state, as is Mn in LMO. Thus Mn in $\mathrm{LaMnO_3}$ and Fe in $\mathrm{CaFeO_3}$ are isoelectronic, i.e., both are in a d^4, $t_{2g}^3\,e_g^1$ state. For Fe d^4, in spite of the orbital degeneracy, the $t_{2g}^3\,e_g^1$ configuration remains free from Jahn-Teller instabilities. They rather show charge-disproportionation transitions [41]. This contrast has been argued by Whangbo *et al.* [42] as followsg: charge disproportionation is favored over JT distortion in $\mathrm{CaFeO_3}$ because the covalent character is strong in the Fe-O bond, while the opposite is true for $\mathrm{LaMnO_3}$ with weaker covalency in the Mn-O bond.

Putting LMO on STO, causes 1.8% compressive strain on LMO, which in turn increases the Mn-O covalency thereby favoring the propensity to charge disproportionation over JT distortion. Allowing the lattice to react to this electronic instability, lowers the symmetry, making Mn1 and Mn2 structurally inequivalent in a $P2_1/n$ monoclinic space group with Mn-O bond lengths at two inequivalent sites differing by about 0.1–0.15 Å, as found in the work by Hou *et al.* [14]. The calculated total energy of the *Pbnm* orthorhombic and $P2_1/n$ monoclinic structures of strained LMO, show the monoclinic structure to be favored by a large energy gain of more than 100 meV/f.u., while DFT + U calculations show only a marginal gain of 6 meV/f.u., as predicted by Hou *et al.* [14]. The heterostructure geometry though is expected to disallow the symmetry-lowering lattice instability. This interesting aspect calls for further investigation.

4. Electronic and magnetic structure: DFT + DMFT

The inability to capture the experimentally observed ferromagnetic insulating state in DFT + U may also stem from a lack of dynamical effects in this computational method. To investigate this possibility, we performed DFT + DMFT calculations. This way we include local dynamical correlations between Mn d-electrons, as well as thermal fluctuations. It is to be contrasted to the hybrid functional which instead improves upon the exchange, which is predominantly nonlocal between the O p and Mn d orbitals.

For unstrained bulk LMO, we capture in DFT + DMFT (at $U = 5$ eV, $J = 0.7$ eV, $\beta = 40$ eV^{-1}, not shown) the correct room temperature paramagnetic phase with an almost complete orbital polarization (97%) of the $x^2 - y^2$ and $3z^2 - r^2$ orbitals, arguably larger than in experiment [43]. Note, however, that our orbitals have a sizable O p admixture and are defined with respect to a local (tilted) coordinate system. As for the bulk magnetic phase occurring at lower temperatures, DFT + DMFT predicts an antiferromagnetic ground state, albeit of G type rather than the experimentally observed A type. One possible reason for this discrepancy might be Hund's exchange on ligand site being neglected. Also the Néel temperature is somewhat larger than the experimental $T_N = 140$ K, as to be expected for a mean-field theory in space which neglects nonlocal spin fluctuations.

Let us now turn to our DFT + DMFT calculations for strained LMO, with the main results shown in Fig. 5. At $J = 0.7$ eV, we find an antiferromagnetic insulator with a net magnetization $M = 0$ and a sizable orbital polarization. This is qualitatively similar as in the unstrained bulk, but quantitatively the strain reduces the Jahn-Teller distortion which in turn reduces the orbital polarization. If we increase J slightly, there is a phase transition to a ferromagnetic metallic phase at $J = 0.9$ eV, signaled by a net magnetization M in Fig. 5. A further increase of Hund's exchange leads to the growth of the local moments as well as the total magnetization, accompanied by a drastic decrease of the orbital polarization. But the ferromagnetic phase remains metallic [44]. Note that a similar increase of the Hund's exchange to $J = 1$ eV for unstrained LMO (not shown) also destroys the antiferromagnetic phase, but neither induces a ferromagnetic phase nor significantly reduces the orbital polarization up to $J = 2$ eV.

We thus conclude that our DFT + DMFT calculations based on a five-orbital d-only model yield a ferromagnet at reasonable values of J, but not a ferromagnetic insulator within a reasonable range of interaction parameters. Local, dynamic correlations within the Mn d manifold are thus not enough to stabilize a ferromagnetic insulating phase.

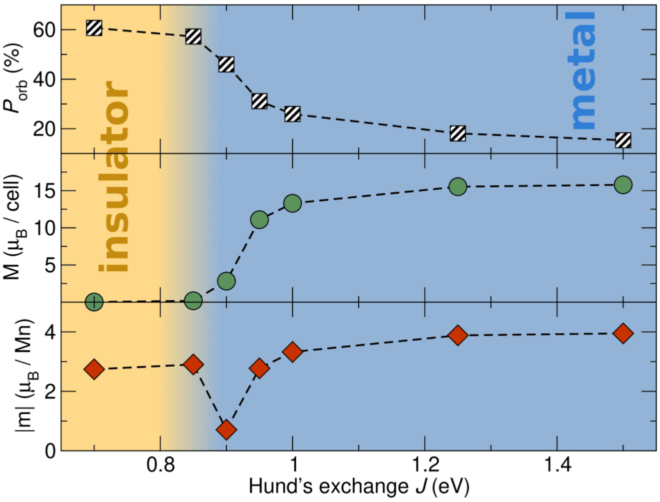

FIG. 5. DFT + DMFT results for strained LMO at 193 K ($\beta = 60$ eV^{-1}) as a function of the Hund's exchange J. The interorbital repulsion $U'(=U-2J)$ is fixed to 3.6 eV. Top, middle, and bottom panels show, respectively, the orbital polarization $P_{\rm orb} = |(n_{3z^2-r^2} - n_{x^2-y^2})/(n_{3z^2-r^2} + n_{x^2-y^2})| \times 100\%$, the total magnetic moment M (in μ_B) per cell, and the absolute value of the ordered moment $|m|$ (in μ_B) averaged over the four Mn sites.

B. LMO/STO superlattice

We next investigate the electronic structure of LMO on STO in the experimental setup, i.e., we consider an actual heterostructure including the STO layers. In addition to the square epitaxial strain of the strained-bulk structure, this in particular involves the polar discontinuity formed between LMO consisting of alternating layers of LaO and MnO$_2$ of +1 and −1 charges and STO consisting of alternating charge neutral layers of SrO and TiO$_2$. The latter would cause half a charge to be transferred between the layers at the interface. Neither the direction nor the extent of this charge transfer has been clarified. The electronic phase separation suggested in recent study [10] is based on the assumption of charge being transferred to LMO, thus doping LMO. To the best of our knowledge, this has not been verified in terms of first-principles calculations or experiment.

For the investigation of the LMO/STO interface as in the experimental situation, we considered superlattice geometry of LMO/STO, with alternate repetition of equal thickness unit cells (4.5) of LMO and STO along the [001] direction, which creates two symmetric n-type interfaces between LaO of LMO and TiO$_2$ layer of STO [5,12]. Equal thicknesses were chosen since the FM insulating state has been experimentally observed for superlattice geometries with nearly equal thickness of LMO and STO layers [12]. The electronic and magnetic structures of the constructed superlattice geometry were investigated within charge self-consistent DFT + U and hybrid functional calculations. The DFT + DMFT calculation became prohibitively expensive for such geometry.

We placed LMO in an orthorhombic geometry matching to square plane STO layers (in the [100] and [010] directions).

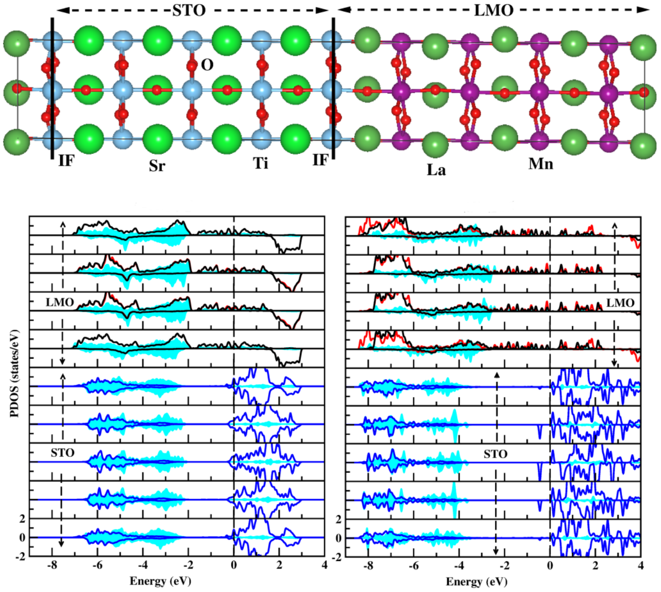

FIG. 6. Top panel: The structure of a $(LMO)_{4.5}/(STO)_{4.5}$ superlattice, projected in the *ac* plane. The large, medium, and small balls represent Sr/La, Ti/Mn, and O atoms, respectively. The interfaces, formed between LaO from LMO and TiO_2 layers from STO, are marked. Bottom panels: Layer projected DOS for a $(LMO)_{4.5}/STO_{4.5}$ superlattice with states projected to Mn1 *d* (black line), Mn2 *d* [red (gray) line], and O *p* [cyan (gray) shaded)] states. The zero of energy is set to the Fermi energy. The left panel shows the DOS calculated in DFT + *U* while the right panel shows the DOS calculated in HSE06 hybrid functional.

Here a $\sqrt{2} \times \sqrt{2} \times c$ supercell of both LMO and STO was allowed to tilt and rotate. This resulted in four Mn and Ti atoms in each MnO_2 and TiO_2 layer, respectively. The ionic positions and *c* lattice parameters were allowed to relax, keeping the constraint of $a = b$ lattice parameters. This setup generates a square matched epitaxial strain of -1.8%, as in previous discussion. The optimized structure shows a significant decrease in Jahn-Teller distortion and modification of tilt and rotation angles in LMO, having a similar trend as in strained-bulk calculation, while some JT distortion and tilt and rotation is introduced in the STO block layers due to its proximity to the largely distorted LMO block, very similar to that found for GTO/STO [5]. The superlattice structure is shown in the top panel of Fig. 6 [45].

Both DFT + *U* and hybrid calculation found the FM magnetic state to be stabilized compared to three different antiferromagnetic structures, i.e., A-AFM, C-AFM, and G-AFM. This again confirms the experimentally observed ferromagnetic state, and is in general agreement with the strained-bulk calculations above.

The bottom, left panel of Fig. 6 shows the layer decomposed partial DOS projected to Mn *d*, Ti *d*, and O *p* in the MnO_2 and TiO_2 layers of LMO and STO blocks, as given in DFT + *U*. We notice the FM electronic state to be half-metallic in each MnO_2 layer of LMO, as found in the DFT + *U* DOS of the strained-bulk structure. The TiO_2 layers are metallic as well, with the Ti *d* states at the interface (IF) TiO_2 layer being spin polarized. This suggests the polar charge to reside within the STO block. This expectation turned out to be true, with the total conduction charge in the STO block to be $1e^-$, being consistent with the presence of two symmetric interfaces in the unit cell, and a carrier density of $0:5e^-$ per IF.

The situation changes dramatically in the hybrid calculation in Fig. 6 (bottom, right), where both LMO and STO blocks are found to be insulating. The charge-disproportionation-driven opening of a band gap is observed in the LMO block, similar to that found in hybrid calculations of the strained-bulk structure. What is very interesting is that the electron gas generated due to polar catastrophe in the STO side becomes fully spin polarized in the TiO_2 layers within the framework of hybrid calculation. The one extra, spin-polarized electron induced by the two *n*-type interfaces is located at the center of the STO block, causing a gap to arise at the Fermi level even in the STO block. This turns the entire system insulating.

IV. SUMMARY AND DISCUSSION

With the aim to provide an understanding regarding the intriguing reports of a ferromagnetic insulating state in LMO/STO heterostructures, we study the problem within a strained-bulk LMO structure using three different theoretical approaches, i.e., DFT + *U*, hybrid functionals, and DFT + DMFT. We find that epitaxial straining to a square substrate of STO results in ferromagnetic ground state in all three approaches, for reasonable choices of parameters. This primarily results from a strong suppression of the JT distortion, which quenches the orbital polarization and hence antiferromagnetism in turn. The electronic state of the strained-bulk structure, however, turned out to be different between the three approaches. DFT + *U* and DFT + DMFT resulted in metallic solution, supporting a double-exchange scenario to be operative. The treatment of exchange effects within a hybrid functional, on the other hand, resulted in an insulating solution. At the microscopic level, the latter is an electronically driven charge disproportionation among the Mn atoms in the unit cell. We note that charge disproportionation is favored over JT distortion in the case of strong metal-oxygen covalency as found in the case of Fe d^4 in $CaFeO_3$ [42], making the propensity to charge disproportionation in the enhanced Mn-O covalency of the strained LMO structure a plausible scenario.

We further investigated the case of the LMO/STO superlattice structure with comparable thicknesses of LMO and STO within the schemes of DFT + *U* and hybrid calculations. As for the strained-bulk structure, it was found that DFT + *U* and hybrid calculations yielded FM metallic and FM insulating states, respectively. In the hybrid functional calculation, the origin of the insulating state in LMO and STO blocks is different: the LMO layers again undergo an electronically driven charge disproportionation, while the latter develop a complete spin polarization and localization of the constituent polar charge.

Our study employing three different, complementary theoretical tools provides an exhaustive description of the problem. Nevertheless, each of the employed methods has limitations that deserve a discussion. First of all, our analysis is restricted to stoichiometric LMO. Possible anionic or cationic defects may have drastic consequences for the electronic and magnetic state, such as admixtures of Mn^{2+} or Mn^{4+} or localization of charge carriers due to disorder. Modeling of such situations, however, requires a better characterization of the experimental samples.

The DFT + U approach is designed to make configurations with larger magnetization favorable by transferring charges between occupied and unoccupied states in the two different spin channels, and thus may not be the best tool to describe the FM insulating state, when starting from a half-metallic solution of DFT. Our DFT + DMFT study is based on the Mn d-only model and has been carried out within the so-called single-shot scheme, or in a noncharge self-consistent scheme. While this incorporates the electronic correlations of the Mn d orbitals, the d-p exchange and a possible charge redistribution due to electronic correlations is neglected. Both effects may turn out to be important for an accurate description of magnetic and electronic state in the presence of strong covalency effects. Furthermore, while local correlations are accounted for in DMFT, nonlocal correlations require cluster [46] or diagrammatic [47] extensions thereof, which are presently unfeasible in our case. Hybrid functionals incorporate a better treatment of the exchange, predominantly between the O p and Mn d states. In our calculation this exchange eventually drives a purely electronic charge disproportionation and opens an insulating gap.

This charge disproportionation of the hybrid functional solution provides at least one route to the experimentally observed ferromagnetic insulator, while we cannot exclude that other effects such as disorder due to cation intermixing or oxygen vacancies also play a role. We conclude that both an improvement of the theoretical approaches, especially considering the effect of electronic correlations on ligand states and their occupation in (charge self-consistent) DFT + DMFT, as well as a better characterization of experimental samples, are needed to have a complete understanding of these complex LMO/STO heterostructures.

ACKNOWLEDGMENTS

H.B. and T.S.-D. thank DST, India, and FWF, Austria for funding support during the execution of the project. Hybrid calculations were performed at computational facilities provided by the Thematic Unit of Excellence on Computational Materials Science, funded by Nano-mission of DST, India at S. N. Bose Centre, Kolkata. O.J. was supported by the Leibniz Association through the Leibniz Competition. DFT+DMFT calculations have been done on the Vienna Scientific Cluster (VSC).

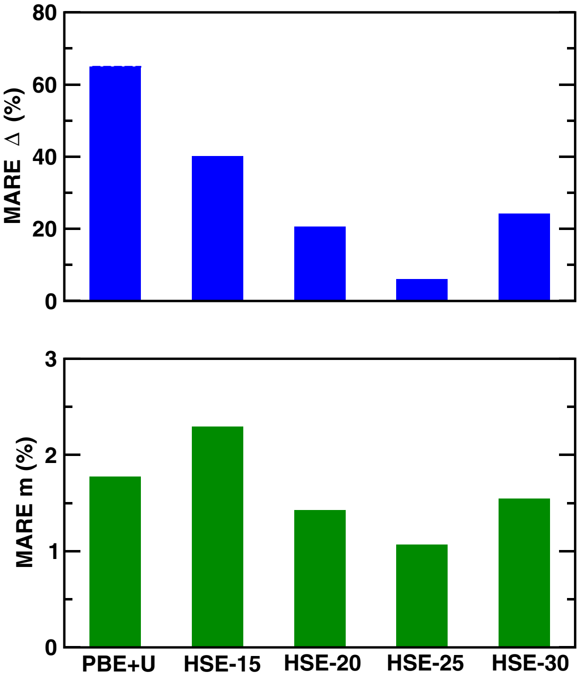

FIG. 7. MARE (%) values for band gaps (top) and magnetic moments (bottom) for different mixing parameters α of the HSE functional. Shown are also DFT + U results.

APPENDIX

For determining the mixing parameter α of the hybrid HSE functional, we compared the calculated band gap and magnetic moment for bulk LMO with experiment. Experimental band gap values of 1.7 [38], 1.9 [48], and 2.0 eV [49,50] have been reported; and experimental magnetic moments were been found to be $3.87\mu_B$ [51] and $3.7\mu_B$ [52]. Here we disregarded the outliers.

To account for the experimental variation, we plot in Fig. 7 the MARE as mentioned in Sec. II. As a percentage, it reads

$$\mathrm{MARE} = \frac{100}{n}\sum_{i=1}^{n}\left|\frac{E_i - T}{E_i}\right|,$$

where E_i represents the experimental value, n the number of experimental values considered, and T the theoretically calculated value for one particular functional.

Figure 7 shows that the MARE is minimal for $\alpha = 0.25$, indicating that $\alpha = 0.25$, rather than $\alpha = 0.15$ [22], provides the best agreement with the experimental band gap and magnetic moment if a higher cutoff for the potential is chosen, at least for $\mathrm{LaMnO_3}$.

---

[1] A. Ohtomo and H. Y. Hwang, Nature (London) **427**, 423 (2004).

[2] S. Gariglio, N. Reyren, A. D. Caviglia, and J.-M. Triscone, J. Phys.: Condens. Matter **21**, 164213 (2009).

[3] P. Moetakef, T. A. Cain, D. G. Ouellette, J. Y. Zhang, D. O. Klenov, A. Janotti, C. G. Van de Walle, S. Rajan, S. J. Allen, and S. Stemmer, Appl. Phys. Lett. **99**, 232116 (2011).

[4] T. A. Cain, P. Moetakef, C. A. Jackson, and S. Stemmer, Appl. Phys. Lett. **101**, 111604 (2012).

[5] H. Banerjee, S. Banerjee, M. Randeria, and T. Saha Dasgupta, Sci. Rep. **5**, 18647 (2015).

[6] J. Garcia-Barriocanal, J. C. Cezar, F. Y. Bruno, P. Thakur, N. B. Brookes, C. Utfeld, A. Rivera-Calzada, S. R. Giblin, J. W. Taylor, J. A. Duffy, S. B. Dugdale, T. Nakamura, K. Kodama,

C. Leon, S. Okamoto, and J. Santamaria, Nat. Commun. **1**, 82 (2010).

[7] J. Garcia-Barriocanal, F. Y. Bruno, A. Rivera-Calzada, Z. Sefrioui, N. M. Nemes, M. Garcia-Hernández, J. Rubio-Zuazo, G. R. Castro, M. Varela, S. J. Pennycook, C. Leon, and J. Santamaria, Adv. Mater. **22**, 627 (2010).

[8] W. S. Choi, D. W. Jeong, S. S. A. Seo, Y. S. Lee, T. H. Kim, S. Y. Jang, H. N. Lee, and K. Myung-Whun, Phys. Rev. B **83**, 195113 (2011).

[9] H. M. Liu, C. Y. Ma, P. X. Zhou, S. Dong, and J.-M. Liu, J. Appl. Phys. **113**, 17D902 (2013).

[10] Y. Anahory, L. Embon, C. J. Li, S. Banerjee, A. Meltzer, H. R. Naren, A. Yakovenko, J. Cuppens, Y. Myasoedov, M. L. Rappaport, M. E. Huber, K. Michaeli, T. Venkatesan, Ariando, and E. Zeldov, Nat. Commun. **7**, 12566 (2016).

[11] X. R. Wang, C. J. Li, W. MThe. Lü, T. R. Paudel, D. P. Leusink, M. Hoek, N. Poccia, A. Vailionis, and T. Venkatesan, Science **349**, 716 (2015).

[12] X. Zhai, L. Cheng, Y. Liu, C. M. Schlepütz, S. Dong, H. Li, X. Zhang, S. Chu, L. Zheng, J. Zhang, A. Zhao, H. Hong, A. Bhattacharya, J. N. Eckstein, and C. Zeng, Nat. Commun. **5**, 4283 (2014).

[13] J. H. Lee, K. T. Delaney, E. Bousquet, N. A. Spaldin, and K. M. Rabe, Phys. Rev. B **88**, 174426 (2013).

[14] Y. S. Hou, H. J. Xiang, and X. G. Gong, Phys. Rev. B **89**, 064415 (2014).

[15] S. L. Dudarev, G. A. Botton, S. Y. Savrasov, C. J. Humphreys, and A. P. Sutton, Phys. Rev. B **57**, 1505 (1998).

[16] J. Heyd, G. E. Scuseria, and M. Ernzerhof, J. Chem. Phys. **118**, 8207 (2003).

[17] V. I. Anisimov, A. I. Poteryaev, M. A. Korotin, A. O. Anokhin and G. Kotliar, J. Phys.: Condens. Matter **9**, 7359 (1997); A. I. Lichtenstein, and M. I. Katsnelson, Phys. Rev. B **57**, 6884 (1998); G. Kotliar, S. Y. Savrasov, K. Haule, V. S. Oudovenko, O. Parcollet, and C. A. Marianetti, Rev. Mod. Phys. **78**, 865 (2006); K. Held, Adv. Phys. **56**, 829 (2007).

[18] P. E. Blöchl, Phys. Rev. B **50**, 17953 (1994).

[19] G. Kresse and J. Hafner, Phys. Rev. B **47**, 558(R) (1993).

[20] G. Kresse and J. Furthmüller, Phys. Rev. B **54**, 11169 (1996).

[21] J. P. Perdew, K. Burke, and M. Ernzerhof, Phys. Rev. Lett. **77**, 3865 (1996).

[22] J. He and C. Franchini, Phys. Rev. B **86**, 235117 (2012).

[23] P. Blaha, K. Schwarz, G. K. H. Madsen, D. Kvasnicka, J. Luitz, R. Laskowski, F. Tran, and L. D. Marks, *WIEN2k, An Augmented Plane Wave + Local Orbitals Program for Calculating Crystal Properties* (Karlheinz Schwarz, Techn. Universität Wien, Austria, 2018).

[24] A. A. Mostofi, J. R. Yates, Y.-S. Lee, I. Souza, D. Vanderbilt, and N. Marzari, Comput. Phys. Commun. **178**, 685 (2008).

[25] J. Kuneš, R. Arita, P. Wissgott, A. Toschi, H. Ikeda, and K. Held, Comput. Phys. Commun. **181**, 1888 (2010).

[26] A. Yamasaki, M. Feldbacher, Y.-F. Yang, O. K. Andersen, and K. Held, Phys. Rev. Lett. **96**, 166401 (2006).

[27] Y.-F. Yang and K. Held, Phys. Rev. B **76**, 212401 (2007).

[28] E. Pavarini and E. Koch, Phys. Rev. Lett. **104**, 086402 (2010).

[29] P. Werner and A. J. Millis, Phys. Rev. B **74**, 155107 (2006).

[30] M. Wallerberger, A. Hausoel, P. Gunacker, A. Kowalski, N. Parragh, F. Goth, K. Held, and G. Sangiovanni, Comput. Phys. Commun. **235**, 388 (2019).

[31] This scheme is often employed in DFT+DMFT calculations of oxide heterostructures when charge self-consistent calculations become prohibitively expensive [32] (see Refs. [33,34] for recent examples).

[32] O. Janson, Z. Zhong, G. Sangiovanni, and K. Held, in *Spectroscopy of Complex Oxide Interfaces*, edited by C. Cancellieri and V. Strocov, Springer Series in Materials Science Vol. 266 (Springer International Publishing, Basel, 2018), p. 215.

[33] O. Janson and K. Held, Phys. Rev. B **98**, 115118 (2018).

[34] S. Beck and C. Ederer, Phys. Rev. Mater. **3**, 095001 (2019).

[35] A. Kowalski, A. Hausoel, M. Wallerberger, P. Gunacker, and G. Sangiovanni, Phys. Rev. B **99**, 155112 (2019).

[36] V. I. Anisimov, I. V. Solovyev, M. A. Korotin, M. T. Czyzyk, and G. A. Sawatzky, Phys. Rev. B **48**, 16929 (1993).

[37] J. Kanamori, Prog. Theor. Phys. **30**, 275 (1963).

[38] T. Saitoh, A. E. Bocquet, T. Mizokawa, H. Namatame, A. Fujimori, M. Abbate, Y. Takeda, and M. Takano, Phys. Rev. B **51**, 13942 (1995).

[39] D. Munoz, N. M. Harrison, and F. Illas, Phys. Rev. B **69**, 085115 (2004).

[40] Such a charge imbalanced state cannot be stabilized within DFT + U or DFT+DMFT, as checked explicitly.

[41] T. Saha-Dasgupta, Z. S. Popović, and S. Satpathy, Phys. Rev. B **72**, 045143 (2005).

[42] M.-H. Whangbo, H.-J. Koo, A. Villesuzanne, and M. Pouchard, Inorg. Chem. **41**, 1920 (2002).

[43] Y. Murakami, J. P. Hill, D. Gibbs, M. Blume, I. Koyama, M. Tanaka, H. Kawata, T. Arima, Y. Tokura, K. Hirota, and Y. Endoh, Phys. Rev. Lett. **81**, 582 (1998).

[44] Interestingly, if we now fix $J = 1.25$eV, which corresponds to 20% orbital polarization with the nearly saturated magnetization (Fig. 5), and increase the interorbital interaction U' from 3.6 to 4.5 eV, the orbital polarization jumps to 66%, while magnetization drops down to $1.9\mu_B$ per cell (not shown).

[45] Structural optimization, starting from monoclinic symmetry of LMO within the superlattice geometry at interface with STO from top and bottom, converged into orthorhombic geometry.

[46] T. A. Maier, M. Jarrell, T. Prushke, and M. Hettler, Rev. Mod. Phys. **77**, 1027 (2005).

[47] G. Rohringer, H. Hafermann, A. Toschi, A. A. Katanin, A. E. Antipov, M. I. Katsnelson, A. I. Lichtenstein, A. N. Rubtsov, and K. Held, Rev. Mod. Phys. **90**, 025003 (2018).

[48] J. H. Jung, K. H. Kim, D. J. Eom, T. W. Noh, E. J. Choi, J. Yu, Y. S. Kwon, and Y. Chung, Phys. Rev. B **55**, 15489 (1997).

[49] J. H. Jung, K. H. Kim, T. W. Noh, E. J. Choi, and J. Yu, Phys. Rev. B **57**, R11043 (1998).

[50] R. Krüger, B. Schulz, S. Naler, R. Rauer, D. Budelmann, J. Bäckström, K. H. Kim, S.-W. Cheong, V. Perebeinos, and M. Rübhausen, Phys. Rev. Lett. **92**, 097203 (2004).

[51] F. Moussa, M. Hennion, J. Rodríguez-Carvajal, H. Moudden, L. Pinsard, and A. Revcolevschi, Phys. Rev. B **54**, 15149 (1996).

[52] J. B. A. A. Elemans, B. van Laar, K. R. van der Veen, and B. O. Loopstra, J. Solid State Chem. **3**, 238 (1971).